Fronts and fluctuations in a tailored model for CO oxidation on metal(100) surfaces

2007 J. Phys.: Condens. Matter 19 065129

(http://iopscience.iop.org/0953-8984/19/6/065129)

INSTITUTE OF PHYSICS PUBLISHING JOURNAL OF PHYSICS: CONDENSED MATTER

J. Phys.: Condens. Matter **19** (2007) 065129 (14pp) doi:10.1088/0953-8984/19/6/065129

Fronts and fluctuations in a tailored model for CO oxidation on metal(100) surfaces

Da-Jiang Liu[1] **and J W Evans**[1,2]

[1] Ames Laboratory—USDOE, Iowa State University, Ames, IA 50011, USA
[2] Department of Mathematics, Iowa State University, Ames, IA 50011, USA

Received 28 August 2006, in final form 6 November 2006
Published 22 January 2007
Online at stacks.iop.org/JPhysCM/19/065129

Abstract

An atomistic lattice-gas model is developed for CO oxidation on unreconstructed metal(100) surfaces. The model is tailored to incorporate the most essential features of such systems: multiple adsorption sites; short-ranged repulsive adspecies interactions; highly mobile CO; and the appropriate Langmuir–Hinshelwood adsorption–desorption and reaction kinetics. The model is applied to analyse both reaction front propagation on extended surfaces and fluctuation phenomena in nanoscale reaction systems. Contrasting conventional ultra-high-vacuum studies, we focus on behaviour at higher pressures or lower temperatures where higher adspecies coverages can result in phase separation of the reactive state into a c(2×2)-O-rich ordered state and an intermixed CO + O state. This phenomenon can produce sharp reaction fronts in extended systems and fluctuation-induced transitions between phase-separated states in nanoscale systems.

1. Introduction

Catalytic oxidation of CO on extended single-crystal surfaces under low-pressure (P) ultra-high-vacuum conditions is perhaps the reaction most studied by the surface science community [1–3]. The Langmuir–Hinshelwood (LH) mechanism for this reaction includes the steps $CO(gas) + * \leftrightarrow CO(ads)$, $O_2(gas) + 2^* \rightarrow 2O(ads)$, and $CO(ads) + O(ads) \rightarrow CO_2(gas) + 2^*$, where gas (ads) denotes a gas-phase (adsorbed) species, and * denotes an empty surface site. Single (double) arrows denote irreversible (reversible) steps. This reaction mechanism produces bistability on an unreconstructed surface provided the surface temperature (T) is not too high [1–3]: a reactive state (with low CO and high O coverage) coexists with an inactive state (with high CO and low O coverage) for a range of CO partial pressures (P_{CO}).

Another feature of these systems is that CO(ads) has high surface mobility with hop rates many orders of magnitude above other rates [4, 5]. In contrast, O(ads) is significantly less mobile. Surface diffusion of CO(ads) coupled with the bistable surface reaction kinetics produces chemical waves or propagating reaction fronts. These fronts separate the two

coexisting stable states in the bistable regime, the more stable state displacing the less stable one. The characteristic front width on the order of microns for low P or high T is controlled by the high chemical diffusivity of CO(ads) [4, 5].

Traditional analyses adopt approximate *textbook chemical kinetics* utilizing mean-field (MF) rate equations to describe CO-oxidation kinetics and steady states, and MF reaction–diffusion equations to describe spatiotemporal behaviour [4]. These MF rate and reaction–diffusion equations assume 'well stirred' (i.e. spatially randomized) reactant adspecies, and also incorporate a simplified description of chemical diffusion on the surface. The inadequacy of this MF picture is discussed below.

Recent interest has expanded to the analysis of catalytic reactions in nanoscale systems such as supported metal clusters [6] and metal field emitter tips (FETs) with facet linear dimensions on the order of $\sim$10 nm [7]. In such systems, fluctuation-induced transitions can occur between the two stable states in the bistable regime [6, 7]. This basic behaviour is captured at least qualitatively by a master equation analysis based on MF kinetics or by corresponding Gillespie-type Monte Carlo simulations [8–10].

The above MF textbook chemical kinetic treatments neglect strong spatial correlations and ordering in the mixed reactant adlayer, which significantly influence reaction kinetics, chemical diffusion within the mixed reactant adlayer, and also fluctuations. It has been long recognized that atomistic lattice-gas (LG) models provide a formulation with the potential to realistically describe such correlations. This approach has been used effectively to provide a realistic characterization of equilibrium structure of single-species adlayers [11] and of temperature-programmed desorption spectra [12]. A long-standing goal has been to extend this approach to rather more complex mixed-adlayer reaction systems. Analysis of these LG models typically would utilize kinetic Monte Carlo simulations. To date, most analysis has been performed on highly idealized models which just incorporate the appropriate LH mechanism [13]. However, such studies neglect many essential features for realistic modelling: multiple adsorption sites for some reactants; strong adspecies interactions producing observed superlattice ordering of adlayer; high mobility of CO(ads) which produces bistability [5, 14], and lower but still significant mobility of O(ads). Only by incorporating all of these features can the model accurately describe spatial correlations and ordering in the reaction system.

Detailed realistic atomistic LG models appropriate for the low-pressure regime have been developed recently for CO oxidation on Pd(100) [15] and Rh(100) [16], and to a lesser extent for Pt(111) [17, 18]. Output from such models has been compared directly with experimental data for temperature programmed desorption spectra and for titration kinetics. One complication is that these models require as input precise values for numerous adspecies binding and interaction energies. One philosophy is that all such energetics should be obtained consistently from density functional theory (DFT) analysis. However, DFT sometimes fails to predict the correct adspecies binding sites, and it should be questioned whether DFT has the accuracy to adequately determine the weaker adspecies interactions which can control adlayer ordering. Alternatively, one can adjust some energetic parameters so that model predictions match experimental observations [15, 16]. However, this approach can also be critiqued. Partly to avoid these problems, and partly because our interest here is in elucidating fundamental and somewhat generic new phenomena, in this paper we explore the behaviour of less system specific and more generic models 'tailored' to capture the essential ingredients of the class of CO oxidation systems of interest.

In section 2, we describe in some detail the key ingredients for realistic models for CO oxidation on unreconstructed metal(100) surfaces, and extract a somewhat simpler and generic 'tailored' model. As indicated above, such a tailored model should be particularly useful for efficient analyses of fundamental phenomena in surface reaction systems. Our focus in this

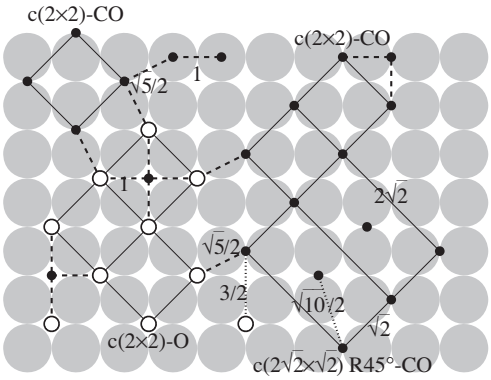

Figure 1. Schematic diagram of adsorption sites, interactions, and ordering for CO(ads) and O(ads). Large grey circles denote the top layer of metal substrate atoms. Small open circles denote O(ads), and small closed circles denote CO(ads). Unit cells for different types of ordering are indicated by thin lines. We also show typical adspecies separations, dashed lines indicating finite repulsion, and dotted lines indicating no interaction.

study is on behaviour at higher P (closing the pressure gap) or lower T than in conventional ultra-high-vacuum studies. In this regime, higher adspecies coverages and associated stronger effects of adspecies interactions are shown to produce phase separation of the reactive state into c(2×2)-O-rich ordered and intermixed CO + O states. In section 4, we explore the consequence for reaction front structure, specifically showing that fronts change from diffuse to atomically sharp with increasing P as a result of phase separation. Then, in section 5, we use the model to explore fluctuation-induced transitions in a nanoscale system. We show that in addition to transitions between reactive and inactive states one can also observe transitions between the c(2×2)-O and intermixed CO + O reactive states for suitably tuned partial pressures. Conclusions are provided in section 6.

2. LG model for CO oxidation on metal(100) surfaces

2.1. Adsorption and interaction energetics

Recently, we have developed *realistic multisite LG models* for CO oxidation on Pd(100) [15] and Rh(100) [16] surfaces for which there is no surface reconstruction. These models include the following key features relating to energetics (see also figure 1):

(i) O(ads) resides only at fourfold hollow (4fh) adsorption sites. Occupancy of nearest-neighbour (NN) sites separated by $d = a$ (where 'a' denotes the surface lattice constant) is effectively excluded due to strong NN repulsions. These produce $(\sqrt{2} \times \sqrt{2})$R45°-O ordering, usually referred to as c(2×2)-O ordering, near 0.5 ML, although behaviour can be complicated by substrate reconstruction. Observed behaviour, including p(2×2) ordering around 0.25 ML, also reflects weaker longer-range interactions [19, 20].

(ii) CO(ads) resides on either bridge (br), 4fh, or on-top (top) sites with different preferences reflecting distinct binding energies [15, 16]. Depending on the system, either br or top sites are most preferred, and here we assume the former (as is the case for Pd). Occupancy of NN bridge sites separated by $d = a/\sqrt{2}$ is excluded. There are significant repulsions between sites separated by a, and various weaker repulsions for more distant pairs of

sites. When the br site is preferred, these interactions can lead to c($2\sqrt{2} \times \sqrt{2}$)R45°-CO ordering [21, 22].

(iii) O(ads)–CO(ads) pairs cannot form with any separation $d < a$ due to strong repulsion. There exist finite repulsions for slightly larger separations. The multisite model allows a realistic description of mixed adlayer structure for the reactive state including phase-separated patches of c(2×2)-O and an intermixed CO + O state.

As noted above and made clear by the above description, these *realistic models* incorporate a large number of parameters associated with adsorption energies and adspecies interactions. Previously, we have selected these with guidance from a density functional theory (DFT) analysis of energetics in order to match experimental observations for various aspects of system behaviour [15, 16]. Here, in developing a *tailored few-parameter model* which captures the essential features of the above realistic models, one might adopt the following simplifications: (i) constrain CO(ads) to its most favourable br site, recalling that O(ads) is already constrained at 4fh sites; and (ii) neglect all adspecies interactions except the exclusions. While such treatments restricting adspecies to their most favourable sites are often adequate to describe single-species systems, they can be woefully inadequate for describing mixed adlayer systems. For example, in the above simple model, a perfect c(2×2)-O adlayer completely blocks adsorption of CO, whereas in reality CO can adsorb at the less favourable 4fh sites.

Thus, to develop a somewhat more realistic *tailored model*, we allow multiple adsorption sites for CO(ads) with a finite binding energy difference, ΔE, between the most favourable (br) and less favourable (4fh, top) ones. We include short-range exclusions, and finite repulsive pairwise interactions for somewhat larger separations as described below. However, to avoid introducing multiple energetic parameters, we also let ΔE correspond to the magnitude of all finite repulsions. Typically, $\Delta E > 0$ is between 0.1 and 0.2 eV. Below, we refer to the associated Boltzmann-type factor $q = \exp[-\Delta E/(k_B T)]$. More specifically, we include the following interactions.

Exclusions. O(ads) is excluded from all br and top sites, and any 4fh site with a NN 4fh O(ads) separated by $d = a$, or any CO(ads) with $d < a$. CO(ads) is excluded from any site with another adsorbate within a distance $d < a$.

Finite repulsions. These exist for (i) O(ads) at 4fh sites with CO(ads) at a separation $d = a$ (4fh) or $d = \sqrt{5}/2a$ (br) and (ii) CO(ads) at br, 4fh, or top sites with any other adsorbate within a distance $a \leqslant d < \sqrt{2}a$.

The total interaction energy for each adsorbate is then ΔE times the total number of neighbours within a distance $d < \sqrt{2}a$. The total interaction energy for the entire system equals half (to avoid double-counting) the sum of these. The total energy associated with binding of CO(ads) to the surface equals $-N_{CO}E_{CO} + N'_{CO}\Delta E$, where $E_{CO} > 0$ is the binding energy at br sites, N_{CO} is the total number of CO(ads) and N'_{CO} is the number of CO(ads) on the less favourable 4fh or top sites.

In our tailored model the only O–O interactions are NN exclusions, but this suffices to produce the observed c(2×2)-O ordering for sufficiently high coverage. For our choice of CO–CO interactions and the preferred br site, one expects a combination of c($2\sqrt{2} \times \sqrt{2}$)R45°-CO ordering and c($2 \times 2$)-CO ordering for coverages approaching 0.5 ML. Perfect ordering for the latter occurs on one-half of the br sites, introducing an extra degeneracy (see figure 1).

2.2. Adsorption–desorption, diffusion, and reaction kinetics

We now specify the dynamics in our tailored model. In treating CO adsorption, we do not include precursor state kinetics or steering effects. Adsorption occurs randomly at available sites of all types (br, 4fh, top) with an equal rate denoted by P_{CO} per site. This rate incorporates

the CO partial pressure and sticking probability. To satisfy detailed balance, desorption of CO has to overcome a barrier $E_{CO} - n\Delta E$. Here, the 'energy level label' n equals the number, N_{int}, of neighbouring adsorbates within $d < \sqrt{2}a$ for br sites, and $n = N_{int} + 1$ for 4fh or top sites. Therefore, the rate for desorption is proportional to q^{-n}. In the following, we denote the rate for the 'typical' local environment with $n = 4$ as d_{CO} so that the general expression for the desorption rate is $d_{CO}q^{4-n}$.

O_2 adsorption is dissociative and described by a modification of the 'eight-site rule' [20, 23]. Due to strong (exclusive) NN O–O repulsions, we require constituent O to adsorb on empty diagonal NN 4fh sites (with $d = \sqrt{2}a$). In addition, these two sites should not be forbidden, meaning they should not have any NN O(ads) (requiring a total of eight sites be free of O(ads) for adsorption), or any CO(ads) within a distance $d < a$. Again, we do not include precursor state kinetics, so O_2 attempts to adsorb randomly at available adsorption site ensembles at a rate denoted by P_{O_2} per site. This rate incorporates the O_2 partial pressure and sticking probability. In the range of temperatures typically used for CO oxidation, oxygen desorption is insignificant. Therefore, O_2 adsorption is treated as irreversible in our modelling.

Diffusion of adspecies is described by hopping between nearby allowed sites with Metropolis-type rates reflecting adspecies interactions. Specifically, we allow hopping between possibly different site types with $d < a$ (for CO), and also between sites of the same type with $d = a$ (for CO or O). The attempt frequency is h_{CO} for CO(ads), and h_O for O(ads). If the hop results in equal or lower energy, it is always accepted. If it results in higher energy, then it is accepted with a probability $\exp[-(E_f - E_i)/(k_B T)]$, where E_i and E_f are the initial and final energies of the total system, respectively. Due to pairwise nature of adspecies interactions, one can write $E_f - E_i = (n_f - n_i)\Delta E$, where n_i and n_f are the initial and final energy levels of the adsorbate, respectively. The acceptance probability is then simply $q^{(n_f - n_i)}$.

As noted in section 1, the hop rate, h_{CO}, for CO(ads) is many orders of magnitude above all other rates. Furthermore, often the hop rate, h_O, for O(ads) is also far above other rates for adsorption, desorption, and reaction (but well below h_{CO}). In this case, the mixed reactant adlayer is in a locally equilibrated Gibbs state, and various properties should be independent of the specific values of the hop rates [24]. Thus, our simulations are typically performed with large equal $h_{CO} = h_O$ ($=h$, say). However, we also comment on behaviour in simulations using large h_{CO} and setting $h_O = 0$.

Finally, we assume that reaction occurs at a common rate k between CO–O pairs separated by $d = a$ (4fh–4fh) and $d = \sqrt{5}a/2$ (br–4fh), noting that repulsive interactions also exist between such pairs [15, 16]. Other prescriptions are also plausible, where the reaction rate depends on the energies of the reacting species.

3. Steady-state behaviour

In this section, we examine the behaviour in our model of the steady-state CO and oxygen coverages versus CO adsorption rate or 'partial pressure' for different total adsorption rates or 'pressures' $P = P_{CO} + P_O$. The curves are obtained using a constant-CO-coverage algorithm [25] which fixes the total number of CO(ads) in the ensemble and calculates the effective P_{CO} to maintain that coverage. Other parameters used here are $k = 1$, $d_{CO} = 0.01$. In this section, we adopt the same value, h, for the hop rates for isolated CO and oxygen.

First, to provide a baseline for interpretation of model behaviour, in figure 2 we show the simple case when $q = 1$, i.e., no adspecies interactions apart from short-range hard-core exclusions. Steady-state coverages exhibit the traditional S-shape behaviour for a bistable LH system. For a range of P_{CO} values, there exist two stable steady states: a reactive state (R) with low θ_{CO} and high θ_O, and an inactive (I) or near-CO-poisoned state with high θ_{CO} and low

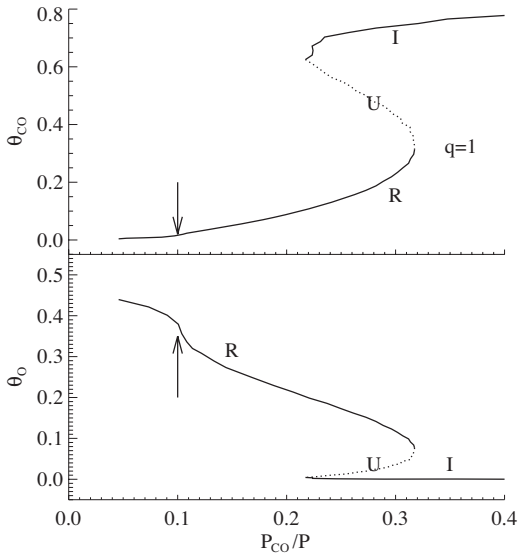

Figure 2. Steady-state coverages of CO and oxygen versus CO partial pressure. Parameters used are $P = 1$, $q = 1$, $k = 1$, $d_{CO} = 0.01$, and $h_{CO} = h_O = h = 10$. Simulations performed on 32×32 system with periodic boundary conditions. Each data point is obtained from averaging over 10^3 time units.

θ_O. These are separated by an unstable steady state (U). In addition and of particular relevance to current study is the occurrence of a continuous phase transition (denoted by an arrow in figure 2) from short-range to long-range c(2×2)-O ordering in the reactive steady state as P_{CO} decreases below about 0.10 and θ_O increases above about 0.35.

The above behaviour including the c(2×2)-O order–disorder transition is very similar to that observed previously in a simpler model, which includes just NN O–O exclusion interactions and where CO resides on the same (4fh) sites as O [26, 27]. Numerical simulations for that simpler model combined with a scaling ansatz [26] demonstrated that the transition is in the universality class of the Ising model.

Qualitative differences emerge in more realistic modelling upon introducing finite longer-range repulsions between CO and oxygen, i.e. choosing $q < 1$ in the model. Simulations below are performed $q = 0.01$ on 32×32 lattice. Other parameters are $k = 1$, $d_{CO} = 0.01$, and $h = 10^4$. Figure 3 shows steady-state behaviour for different total pressures P.

For $P = 0.1$, the reactive branch of the steady state exhibits a second small S-shaped loop (effectively replacing the non-analytic feature at the continuous transition for $q = 1$). This loop indicates a discontinuous transition in the reactive steady state between a long-range c(2×2)-O ordered phase and a disordered phase where CO and O are intermixed. The transition occurs with θ_O varying from about 0.32 to 0.38 and for very low θ_{CO}. As P increases further to around 1, the loop corresponding to the discontinuous transition in the reactive phase expands over a broader coverage range, and shifts to the regime with higher θ_{CO} and lower θ_O. Finally, as P increase further to 10, only the reactive phase with ordered c(2×2)-O remains stable.

It is appropriate to comment further on the nature of the reactive steady states resulting from phase separation. Of particular note is the intermixed reactive phase which includes finite CO-rich blobs and O-rich blobs, the size of which is determined by the relative magnitude of the hop rate and the reaction rate. This is truly a nonequilibrium steady state distinct in character from states in equilibrium systems undergoing phase separation where blobs coarsen indefinitely. Finally, in contrast, we note that the long-range c(2×2)-O ordered phase is similar to analogous equilibrium phases.

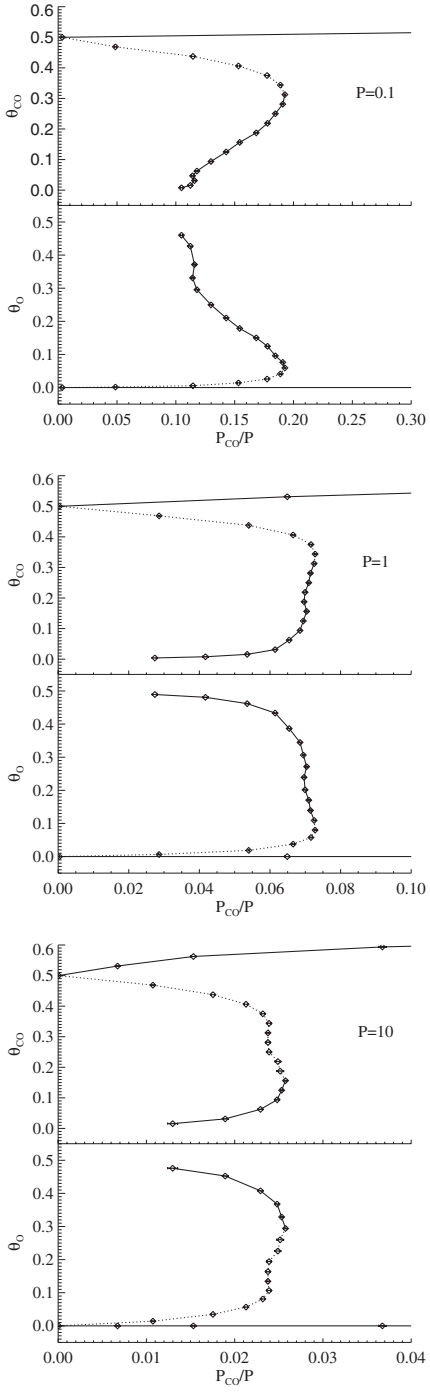

Figure 3. Steady-state coverages of CO and oxygen versus CO partial pressure for different total pressure P. Other parameters are $q = 0.01$, $k = 1$, $d_{CO} = 0.01$, and $h_{CO} = h_O = h = 1000$. Simulations performed on 32×32 system with periodic boundary conditions. Each data point is obtained from averaging over 10^4 time units.

The above steady-state curves were obtained for a finite $L \times L$ system using a 'moderate' hopping rate h for CO and oxygen. How does behaviour change for much larger L and/or h? In the limit $L \to \infty$, with fixed finite h, the unstable portion of the steady-state curve

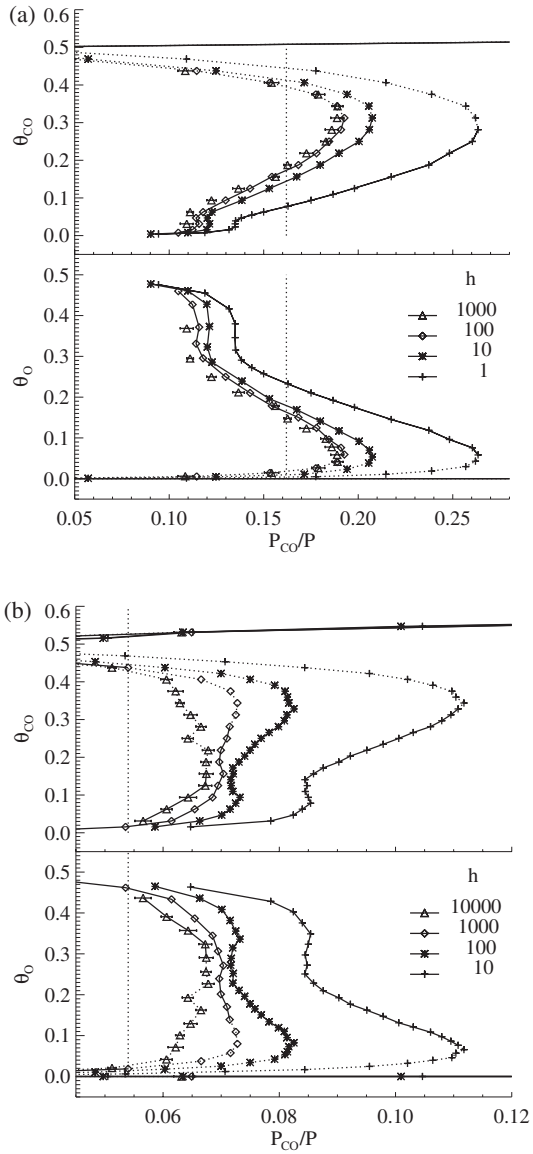

Figure 4. Steady-state coverages of CO and oxygen versus CO partial pressure for different adspecies hopping rates h. (a) $P = 0.1$; (b) $P = 1$. The vertical dotted lines indicate the LH equistability pressures for $h = 100$ in (a) and $h = 10^5$ in (b). See section 4 for details.

(where the P_{CO}–θ_{CO} curve has negative slopes) associated with phase separation of the reactive state tends to becomes more vertical. The corresponding P_{CO} value corresponds to the 'phase-separation (PS) equistability' pressure for these reactive states. In principle, the same applies for the unstable state associated with bistability in the LH mechanism. However, high CO hop rates (see below) make this bistability quite robust.

Typically, the diffusion barrier for CO on metal surfaces is small, perhaps around 0.2 eV [15]. This corresponds to a very high CO hop rate, e.g., $h_{CO} \sim 10^9$ s^{-1} at room temperature. The diffusion barrier for O is significantly higher [20], resulting in lower hop rates, perhaps $h_O \sim 10^3$ s^{-1} at room temperature. Since it is impractical to simulate the process with h much above 10^4, we perform simulation with various smaller values and extrapolate behaviour to large h. Figure 4 shows the steady-state coverage versus P_{CO} curves for different

h at $P = 0.1$ and 1. For $P = 0.1$, the curves rapidly converge as h increases above 100. However, for $P = 1$, no convergence is apparent for the range of h considered, with the curves even changing qualitatively as h increases from 10^3 to 10^4. In summary, for the low-P regime, one can use simple extrapolation to readily determine large-h hydrodynamic behaviour. However, in the regime of higher P, such simple extrapolation procedures are not adequate.

The lack of convergence for higher P can be rationalized by noting that for the intermixed CO + O reactive state generated by phase separation, the size of the blobs of CO and O increases with increasing h. If these blobs are smaller than the system size (e.g. for $h = 10^3$), then the state is stable. However, when they become comparable to or larger than the system size (e.g. for $h = 10^4$), then this state becomes unstable.

Finally, we have noted above that the oxygen hopping rate is typically large, but significantly smaller than that for CO. Thus, in addition to the above simulations setting $h_{CO} = h_O = h$, it is instructive to investigate the limiting case where O(ads) is entirely immobile. Simulations with $h_O = 0$ show no qualitative difference from the case $h_O = h_{CO}$ studied above. The system exhibits the same discontinuous phase transition, although the metastability and hysteresis are weaker.

4. Diffuse versus sharp reaction fronts in a bistable reaction system

Photo-emission and low-energy electron microscopy studies of CO oxidation on single-crystal surface under ultra-high vacuum conditions reveal expected behaviour for bistable reaction–diffusion systems, i.e. propagation of chemical or trigger waves corresponding to the interface between the reactive and inactive states [4]. Usually, there is a unique value of the partial pressure P_{CO}, where the reactive and inactive states are equally stable and the front is stationary. We describe this as the LH-equistability pressure to distinguish it from the distinct PS-equistability pressure described in section 3 and associated with phase separation. Under conditions of low P and weak effective adspecies interactions, the chemical diffusion rate is proportional to the (very high) CO hopping rate. The characteristic width and velocity of the reaction front scale as $h_{CO}^{1/2}$ [4, 5]. The width is on the order of microns.

Direct numerical study of the atomistic model on such a large spatial scale and for such high CO hop rates is of course impossible. However, two alternative strategies can be applied based on the existence of the hydrodynamic scaling mentioned above and exact non-MF reaction–diffusion equations [5].

(i) One can perform simulations for a reduced hop rate and then simply scale up the results for front profile and propagation velocity using the above scaling relationship. This is a straightforward but 'brute force' approach.

(ii) One can implement an equation-free heterogeneous multiscale modelling approach, 'heterogeneous-coupled-lattice-gas' (HCLG) simulation, in which one performs parallel simulations of the reaction at points distributed across the front and suitably coupled to reflect mesoscopic CO surface diffusion [14, 28]. Key input to the HCLG analysis is a precise determination of the chemical diffusivity of CO in mixed interacting reactant adlayers [24]. This HCLG formulation has been implemented for realistic atomistic models [24, 29], providing more insight into behaviour than the rescaling approach.

Here, we first present results for behaviour from the brute force scale-up approach for the *low* P regime. Figure 5 shows the profile of the interface with $P = 0.1$, $h = 100$, $q = 0.01$ and $d_{CO} = 0.01$ at the LH-equistability pressure $P_{CO}/P = 0.162$. Results are obtained from constant CO-coverage simulations with $L = 512$. By starting with a strip of the inactive CO-poisoned state, we ensure that a CO partial pressure near the LH equistability condition is

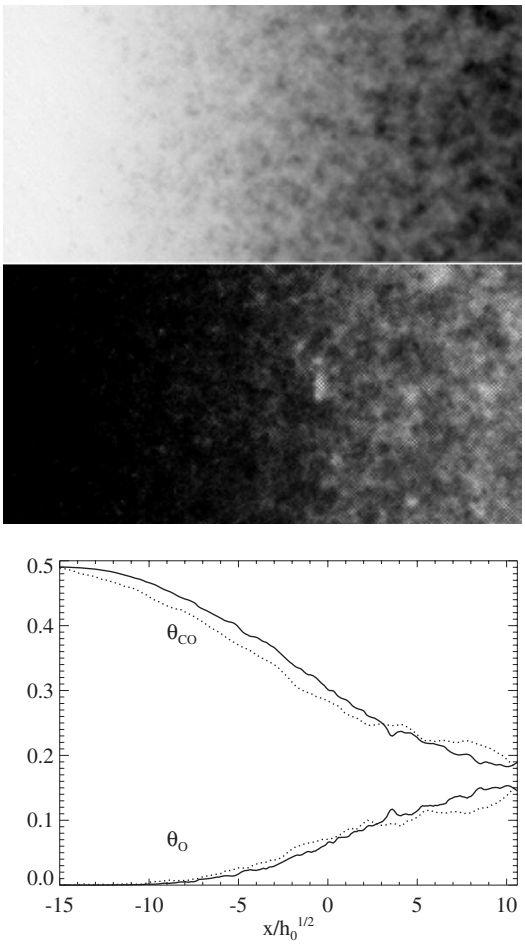

Figure 5. Planar interface between reactive and non-reactive phases for $P = 0.1$, $h = 100$, $q = 0.01$, and $d_{CO} = 0.01$, near LH-equistability where the interface is stationary. Results are obtained from a constant-θ_{CO} simulation with $P_{CO}/P = 0.162$ (cf figure 4). The upper panel shows a grey-scale image of coverages averaged over 100 time units in a system of size 256×256 sites split so the top half (bottom half) shows CO (oxygen). Brighter images corresponds to higher coverages. The lower panel shows the coverage profiles averaged over the y-direction orthogonal to the front. The x-axis is scaled by $h^{-1/2}$. The solid line is for $h = 100$, and the dotted line is for $h = 10$.

automatically selected. For this pressure, the reaction front connects the CO poisoned phase to the intermixed reactive phase. Behaviour is averaged over 100 time units, which smears out atomic motion but preserves nanoscale structure. In fact, the system is highly inhomogeneous on the nanoscale with the reaction front consisting of patches of CO and oxygen, although these are quite mobile. Averaging over these inhomogeneities (either on a longer timescale for a narrow portion of the front, or spatially averaging over a sufficiently wide portion), one obtains a coverage profile which varies smoothly from one phase to the other, as shown in figure 5.

Next, we consider the regime of *higher* P, where quite distinct behaviour applies. Even for $P = 1$, the analysis of figure 4 indicates that the hydrodynamic description breaks down for steady-state behaviour. It is clear from this figure that for large enough h there is effectively

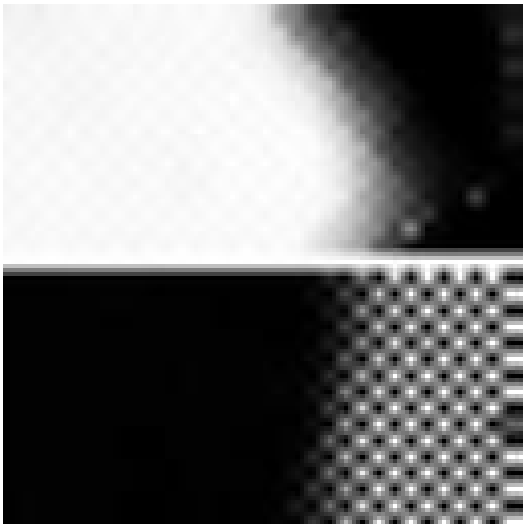

Figure 6. Interface between reactive and inactive phases for $P = 1$ and $h = 10^5$, $q = 0.01$, and $d_{CO} = 0.01$ near LH-equistability where the interface is stationary. Results are obtained from a constant-θ_{CO} simulation with $P_{CO}/P = 0.054$ (cf figure 4). A grey-scale image of coverages averaged over ten time units in a system of size 32×32 sites split so the top half (bottom half) shows CO (oxygen). Brighter images correspond to higher coverages.

phase separation between the inactive CO-poisoned phase and the c(2×2) ordered oxygen-rich reactive phase. Any reaction front will span these states. A consequence is the breakdown of hydrodynamic scaling behaviour with respect to the CO hopping rate for the reaction-front profile.

Figure 6 shows the stationary reaction front profile for $P = 1$, $h = 10^5$, $q = 0.01$ and $d_{CO} = 0.01$, obtained from constant-CO-coverage simulations with $L = 64$. The front is atomically sharp; its width does not scale as $h^{1/2}$. Furthermore, front dynamics is quite distinct from that of a diffuse front. Large fluctuations of the front predominate. Also, many small patches of CO in the reactive phase, and of oxygen in the inactive phase, constantly move in and out of the interface. As an aside, we note that the correlation between sharp fronts in an adsorption–desorption system, and adspecies interactions which produce a discontinuous phase transition have been explored within a simple mean-field framework [30]. Of course, sharp fronts within near-equilibrium equilibrium systems displaying discontinuous phase transitions have been explored extensively and are usually referred to as phase waves [31].

The above examples are for behaviour of near-stationary reaction fronts. The picture for propagating reaction fronts can be more complicated. More specifically, unusual features derive from the occurrence of distinct CO partial pressures for equistability of inactive and reactive states ($P_{CO} = P_{LH}$) and for phase separation in the reactive state ($P_{CO} = P_{PS}$). *First*, consider low $P = 0.1$ where $P_{PS} < P_{LH}$ from figure 4, and select $P_{CO} < P_{PS} < P_{LH}$. Starting from a sharp interface between the ordered oxygen-rich reactive phase and the inactive CO-poisoned phase, two fronts can develop: one is an extended front separating the intermixed reactive phase propagating into the CO-poisoned phase; the other is a sharp front separating the oxygen-rich reactive phase propagating into the intermixed reactive phase. See figures 7 and 8. *Second*, consider higher $P = 1$ where $P_{LH} < P_{PS}$ from figure 4, and select $P_{LH} < P_{CO} < P_{PS}$. Starting from a sharp interface between the ordered oxygen-rich reactive phase and the inactive CO-poisoned phase, the interface remains sharp but fluctuates strongly. Blobs of the inactive state are randomly nucleated in the less stable reactive state. Rather than growing, they diffuse rapidly (at least for large h) and attach to the nearby interface, resulting in strongly fluctuating propagation of the inactive state into the reactive state.

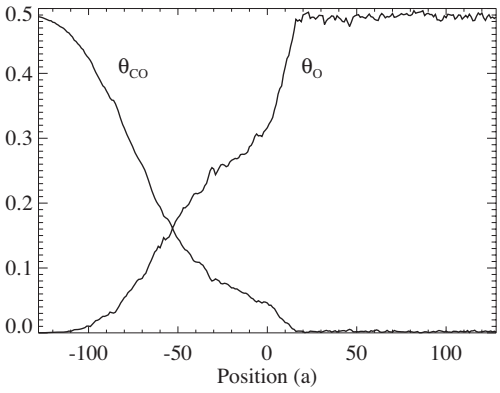

Figure 7. Propagating interface profile between reactive and inactive phases for $P = 0.1$, $h = 10$, $q = 0.01$, and $d_{CO} = 0.01$. Results are obtained from standard simulations with $P_{CO} = 0.1P$, starting with a sharp interface. The system size is 512×512.

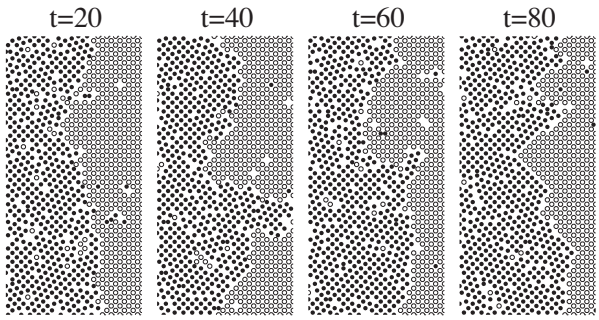

Figure 8. Propagating planar interface between reactive and inactive phases for $P = 1$, $h = 10^5$, $q = 0.01$, and $d_{CO} = 0.01$. Results are obtained from standard simulations with $P_{CO} = 0.065P$, starting with a sharp interface. The size of the system shown is 32×64.

5. Fluctuations and patterns in nanoscale systems

Studies of surface reactions in confined nanoscale systems such as metal field emitter tips (FETs) [7], and supported metal clusters, which are of particular industrial relevance [6], have received much recent attention. A major advantage of studies on FETs is that one can use field-ion or field-emission microscopy to monitor the spatial–temporal behaviour of the reactants in real-time and with near-atomic resolution. A fairly complete analysis of mean-field (MF) type behaviour for lower P has been developed [9, 32]. Rather different behaviour can occur at higher P due to the stronger effects of adspecies interactions at higher reactant coverages.

First, we illustrate traditional MF-type behaviour for fluctuation-induced transitions in a small bistable reaction system at lower P or higher temperature (i.e., q close to unity). Here, the transition is between two *homogeneous* phases, and the system makes the transition in a spatially concerted or coherent fashion, as shown in the upper portion of figure 9 for $P = 1$, $q = 1$, and $h = 100$. Thus, time series for the CO coverage in a subwindow shown in the lower portion of figure 9 (mimicking procedures used to monitor behaviour in FET studies) produces behaviour similar to that for the entire system. One characteristic of such an MF-type transition is that the waiting time is very sensitive to the system size. One can show that for a system with periodic boundary conditions, in the limit of very large h, the waiting time is proportional to $\exp(\alpha L^2)$ [9].

Contrasting the above MF-type behaviour, figure 10 shows the real-space configurations from a simulation on a 32×32 system with $P = 1$, $q = 0.01$, and $h = 10^3$. The CO partial pressure is chosen at 0.071, close to where the reactant phase separation occurs with these parameters (cf figures 3 and 4). In addition, in figure 10, we show the time series for the

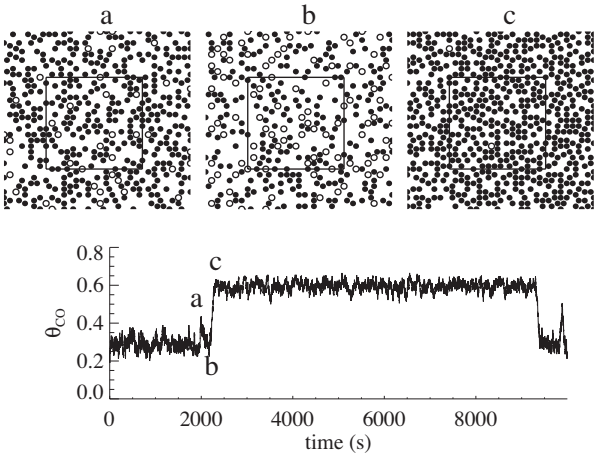

Figure 9. Upper panel: full real-space configurations for a 32×32 system during CO oxidation for $P = 1$ and $q = 1$. Other parameters are $P_{CO} = 0.335$, $h = 10^2$, $k = 1$ and $d_{CO} = 0.03$. Open circles are for oxygen and closed circles are for CO. Lower panel: time series for the CO coverage taken from the subwindow indicated by the square in the upper panel. Times when the snapshots are taken are indicated by the letters.

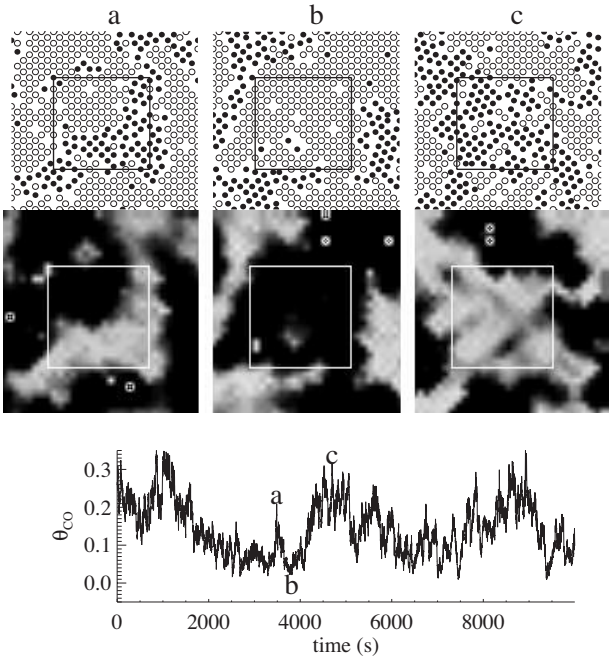

Figure 10. Upper panels: full real-space configurations and grey-scale images of CO coverages of a 32×32 system during CO oxidation for $P = 1$ and $q = 0.01$. Other parameters are $P_{CO} = 0.071$, $h = 10^3$, $k = 1$, $d_{CO} = 0.01$. Open circles are for oxygen and closed circles are for CO. Lower panel: time series for the CO coverage taken from the subwindow indicated by the square in the upper panel. Times when the snapshots are taken are indicated by the letters.

CO coverage obtained from a 16×16 subwindow, again mimicking procedures used to monitor behaviour in FET studies. Large fluctuations are apparent. The system consists of CO-rich and O-rich patches frequently moving in and out of the subwindow. Now, there are two contributing mechanisms for large changes in subwindow coverages: one is due to one particular CO- or O-rich patch shrinking or growing; the other is due to the patches diffusing in and out of the subwindow. Overall behaviour can be described as 'flickering' of the images.

6. Conclusions

We have developed a tailored multisite LG model which effectively captures the behaviour of CO oxidation on unreconstructed metal(100) surfaces. This tailored model allows more effective and comprehensive analysis of fundamental issues related to steady-state behaviour and its dependence on model parameters (particularly adspecies hop rates), front propagation, and nanoscale fluctuations. The enhanced efficiency of the tailored model, versus more complete realistic models, is particularly important for our analyses of behaviour at higher P where simple hydrodynamic scaling does not apply. In particular, we are able to elucidate some novel consequences of reactant phase separation due to the effects of adspecies interactions for higher reactant coverages associated with higher P.

Acknowledgments

This work was supported by the Division of Chemical Sciences of the US Department of Energy (Basic Energy Sciences). It was performed at Ames Laboratory, which is operated for the USDOE by Iowa State University under contract No W-7405-Eng-82.

References

[1] Engel T and Ertl G 1979 *Adv. Catal.* **28** 1
[2] Ertl G 1991 *Adv. Catal.* **37** 213
[3] Imbihl R 1993 *Prog. Surf. Sci.* **44** 185
[4] Imbihl R and Ertl G 1995 *Chem. Rev.* **95** 697
[5] Evans J W, Liu D-J and Tammaro M 2002 *Chaos* **12** 131
[6] Johánek V, Laurin M, Grant A W, Kasemo B, Henry C R and Libuda J 2004 *Science* **304** 1639
[7] Suchorski Y, Beben J, James E W, Evans J W and Imbihl R 1999 *Phys. Rev. Lett.* **82** 1907
[8] Suchorski Y, Beben J, Imbihl R, James E W, Liu D-J and Evans J W 2001 *Phys. Rev.* B **63** 165417
[9] Liu D-J and Evans J W 2002 *J. Chem. Phys.* **117** 7319
[10] Pineda M, Imbihl R, Schimansky-Geir L and Zülicke C 2006 *J. Chem. Phys.* **124** 044701
[11] Weinberg W H 1983 *Annu. Rev. Phys. Chem.* **34** 217
[12] Jansen A P J 2004 *Phys. Rev.* B **69** 035414
[13] Ziff R M, Gulari E and Barshad Y 1986 *Phys. Rev. Lett.* **56** 2553
[14] Tammaro M, Sabella M and Evans J W 1995 *J. Chem. Phys.* **103** 10277
[15] Liu D-J and Evans J W 2006 *J. Chem. Phys.* **124** 154705
[16] Liu D-J 2006 unpublished
[17] Völkening S and Wintterlin J 2001 *J. Chem. Phys.* **114** 6382
[18] Petrova N V and Yakovkin I N 2005 *Surf. Sci.* **578** 162
[19] Chang S-L and Thiel P A 1988 *J. Chem. Phys.* **88** 2071
[20] Liu D-J and Evans J W 2004 *Surf. Sci.* **563** 13
[21] Behm R J, Christmann K, Ertl G and Van Hove M A 1980 *J. Chem. Phys.* **73** 2984
[22] Liu D-J 2004 *J. Chem. Phys.* **121** 4352
[23] Chang S-L and Thiel P A 1987 *Phys. Rev. Lett.* **59** 296
[24] Liu D-J and Evans J W 2006 *J. Chem. Phys.* **125** 054709
[25] Ziff R M and Brosilow B J 1992 *Phys. Rev.* A **46** 4630
[26] Liu D-J and Evans J W 2000 *Phys. Rev. Lett.* **84** 955
[27] James E W, Song C and Evans J W 1999 *J. Chem. Phys.* **111** 6579
[28] Liu D-J and Evans J W 2005 *Multiscale Modelling Simul.* **4** 424
[29] Liu D-J and Evans J W 2004 *Phys. Rev.* B **70** 193408
[30] Mikhailov A and Ertl G 1995 *Chem. Phys. Lett.* **238** 104
[31] Gunton J D, Miguel M S and Sahni P S 1983 *Phase Transitions and Critical Phenomena* vol 8 (New York: Academic)
[32] Liu D-J, Pavlenko N and Evans J W 2004 *J. Stat. Phys.* **114** 101